Neodymium isotope constraints on provenance, dispersal, and climate-driven supply of Zambezi sediments along the Mozambique Margin during the past ~45,000 years

H. J. L. van der Lubbe[1,2], Martin Frank[3], Rik Tjallingii[4,5], and Ralph R. Schneider[1]

[1]Marine Climate Research, Institute of Geosciences, University of Kiel (CAU), Germany, [2]Now at Department of Sedimentology and Marine Geology, Faculty of Earth and Life Sciences, Vrije Universiteit Amsterdam, Netherlands, [3]GEOMAR Helmholtz Centre for Ocean Research, Kiel, Germany, [4]Department of Marine Geology, NIOZ - Royal Netherlands Institute for Sea Research, Texel, Netherlands, [5]Now at GFZ - German Research Centre for Geosciences, Potsdam, Germany

Abstract Marine sediments deposited off the Zambezi River that drains a considerable part of the southeast African continent provide continuous records of the continental climatic and environmental conditions. Here we present time series of neodymium (Nd) isotope signatures of the detrital sediment fraction during the past ~45,000 years, to reconstruct climate-driven changes in the provenance of clays deposited along the Mozambique Margin. Coherent with the surface current regime, the Nd isotope distribution in surface sediments reveals mixing of the alongshore flowing Zambezi suspension load with sediments supplied by smaller rivers located further north. To reconstruct past changes in sediment provenances, Nd isotope signatures of clays that are not significantly fractionated during weathering processes have been obtained from core 64PE304-80, which was recovered just north of the Zambezi mouth at 1329 m water depth. Distinctly unradiogenic clay signatures (ε_{Nd} values < -14.2) are found during the Last Glacial Maximum, Heinrich Stadial 1, and Younger Dryas. In contrast, the Nd isotope record shows higher, more radiogenic isotope signatures during Marine Isotope Stage 3 and between ~15 and ~5 ka BP, the latter coinciding with the timing of the northern hemisphere African Humid Period. The clay-sized sediment fraction with the least radiogenic Nd isotope signatures was deposited during the Holocene, when the adjacent Mozambique Shelf became completely flooded. In general, the contribution of the distinctly unradiogenic Zambezi suspension load has followed the intensity of precession-forced monsoonal precipitation and enhanced during periods of increased southern hemisphere insolation and high-latitude northern hemispheric climate variability.

1. Introduction

The African monsoonal precipitation belt migrates latitudinally during the year, thereby causing seasons of maximum precipitation over tropical Africa [e.g., *Nicholson*, 2000]. How this precipitation belt has varied in strength and position under past climate conditions at high and low latitudes is still a matter of debate, particularly for southeast Africa. Here terrestrial proxy records of hydrological conditions during the Holocene and Pleistocene are scarce and do not provide a coherent signal. Large part of this uncertainty can be attributed to hiatuses, geochronological issues, and geographical effects on the distribution and intensity of precipitation [e.g., *Garcin*, 2008; *Stager et al.*, 2011]. In contrast, marine records, particularly those situated near large river mouths, can provide continuous, high-resolution proxy records for the environmental and climatic conditions on the adjacent continent. In addition, radiocarbon dating of terrestrial records is often hampered by hardwater effects making direct comparison to marine climate records difficult. The Zambezi River, which drains the largest catchment area on the South African continent, discharges sediment to the Mozambique Channel which is part of the western limb of the southern Indian Ocean circulation. The Zambezi Catchment is situated in the southernmost reach of the African monsoonal precipitation belt. Peak precipitation in the upstream areas of the Zambezi Catchment (i.e., upstream the Victoria Falls) is controlled by the seasonal migration of the Congo Air Boundary (CAB), which separates the Indian and Atlantic Ocean air masses (Figures 1a and 2). Precipitation originates predominantly from the Atlantic Ocean via extensive recycling of moisture over southwestern Africa. In the lower catchment areas, maximum precipitation
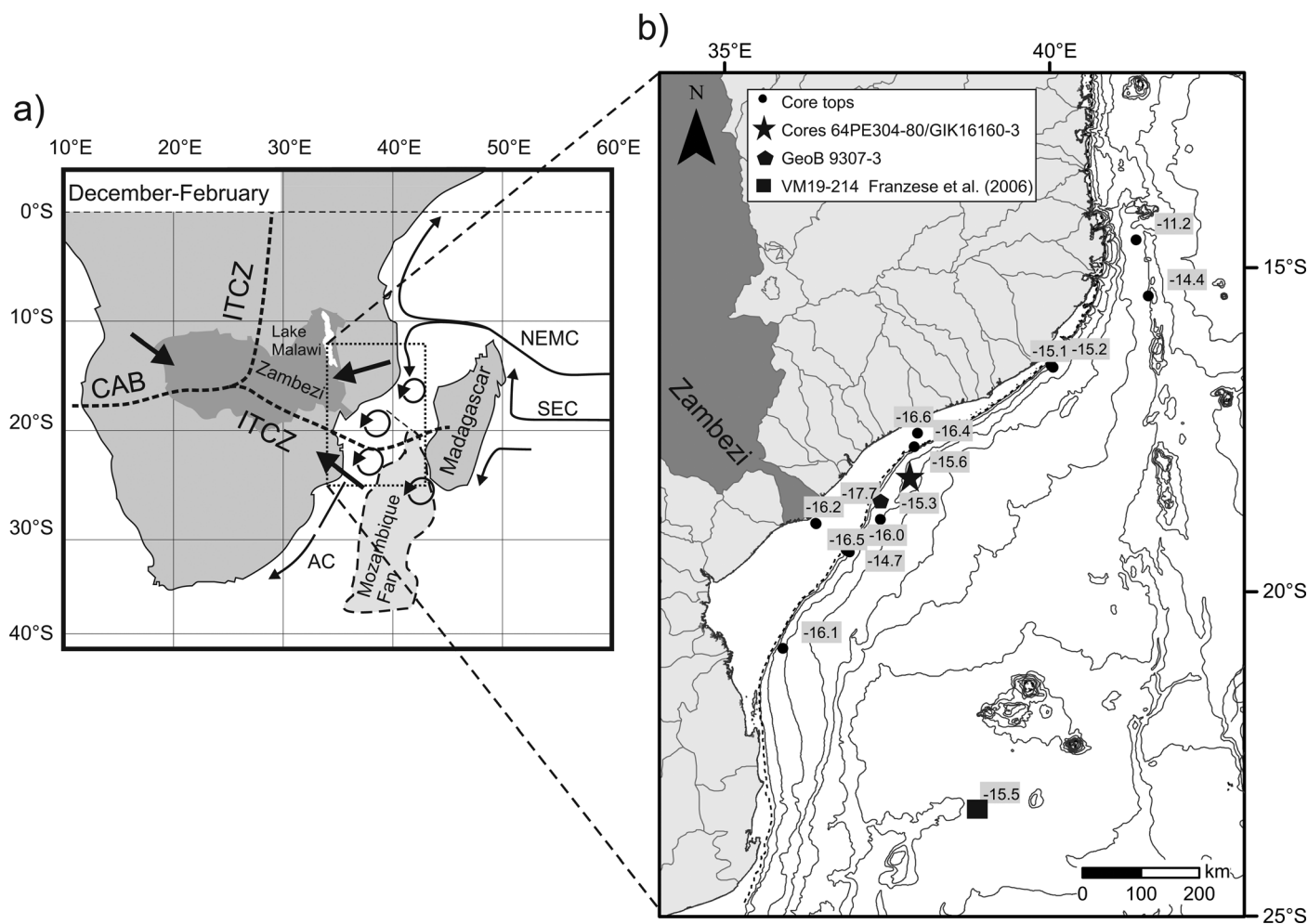
Figure 1. (a) Schematic map of southeast Africa shows the major atmospheric boundaries (dashed lines; adapted from *Reason et al.* [2006]) during austral summer (December–February) and main surface currents (solid thin arrows) in the adjacent southwest Indian Ocean (adapted from *van der Lubbe et al.* [2014]). The Zambezi Catchment that includes Lake Malawi is indicated by the dark shaded area. The large thick arrows indicate the main pathways of moisture supply to the African continent from the NW Atlantic (via Congo), the NE, and the SE Indian Ocean. The South Equatorial Current (SEC) splits into the Northeast Madagascar Current (NEMC) approaching the Madagascar, which feeds in turn the net southward flow through the Mozambique Channel (MC). The flow through the Mozambique Channel occurs through the passage of large anticyclonic eddies, which occasionally continue into the Agulhas Current (AC) [*Ridderinkhof et al.*, 2010]. Sediments are mainly transported in southward direction and deposited onto the large Mozambique deep-sea fan, which is marked in light gray [*Kolla et al.*, 1980a,b]. (b) A detailed map of study area that is outlined by a dashed rectangle in Figure 1a displays the surface distribution of ε_{Nd} values in clay-sized lithogenic sediments in the Mozambique Channel. The core site of cores 64PE304-80 and GIK16160-3 as well as core GeoB9307-3 are indicated by a star and pentagon, respectively. River catchments are delineated by thin black lines, whereas the Zambezi Catchment is indicated by the dark shaded area. Depth contours are drawn at 500 m intervals and the shelf-break is approximated by a dashed line following the contour of 100 m depth water.

occurs when the African precipitation belt, associated with the Intertropical Convergence Zone (ITCZ), migrates in concert with the CAB to the northern half of the Zambezi Catchment during austral summer (December–February) [*Moore et al.*, 2008] (Figure 1a). Thus, the Zambezi Catchment is a key area for reconstructing monsoonal precipitation variability related to shifts in these major atmospheric boundaries. Marine sediment cores recovered near the Zambezi mouth have the potential to provide comprehensive proxy records that recorded changes in hydrological conditions of the African precipitation belt in southeastern Africa [*Just et al.*, 2014; *Schefuss et al.*, 2011; *Wang et al.*, 2013].

Previous paleoclimate studies on Mozambique Margin sediments have focused on proximal sediment cores near the Zambezi mouth, locations sensitive to near-coast sedimentary processes. Here sediment deposition is strongly affected by glacial-interglacial sea level variations, which shifted the main sediment transport pathways [*van der Lubbe et al.*, 2014]. The locations of seafloor depocentres for fine-grained fluvial sediments shifted over time, which can be problematic when attempting to use proxies at isolated core locations to reconstruct climatic and environmental changes in the adjacent catchment areas [*Just et al.*, 2014;

Weldeab et al., 2014]. However, the lithogenic fraction of deep-sea sediment itself carries important information on these changes, as well as on the mechanisms by which material is transported from land to the deep sea. Clay minerals are of particular interest, since they are a significant constituent of seafloor sediments and can be transported over long distances. Moreover, radiogenic isotope signatures of detrital clays in marine sediments are a well-established indicator to reconstruct changes in sediment source areas (i.e., geographical provenances) and have been related to past climatic and hydrographic changes [e.g., *Franzese et al.*, 2006; *Grousset et al.*, 1992; *Stumpf*, 2011].

Compared to other radiogenic isotope systems (such as Sr, Pb, and Hf), the neodymium isotope (ε_{Nd}) signatures are essentially unaffected by particle size and do not fractionate significantly during chemical weathering [e.g., *Jung et al.*, 2004; *Meyer et al.*, 2011]. Instead the detrital particles formed reflect the initial ε_{Nd} signatures and crustal age of their source rocks [e.g., *Goldstein et al.*, 1984]. It is in particular the bedrock composition and weathering intensity of large rivers that may vary spatially across the drainage basins. The clay-sized fraction is transported over large distances through the different riverine catchment areas (Figure 2) and, therefore, integrates the ε_{Nd} signatures of the diverse bedrock types and ages in the source areas. The analysis of ε_{Nd} signatures of lithogenic fractions in marine sediments is a powerful and widely applied tool to asses variations of sediment provenance and transport. For example, the ε_{Nd} signatures of the fine-grained detrital fraction in marine sediments recovered near the Nile delta document varying proportions of sediments originating from White and Blue Nile subcatchments [*Blanchet et al.*, 2014, 2013; *Revel et al.*, 2010]. For the Congo [*Bayon et al.*, 2012] and Orange [*Weldeab et al.*, 2013] rivers, the ε_{Nd} of the lithogenic fraction allowed the reconstruction of climate and precipitation-driven changes in sediment provenance. Radiogenic isotopes signatures including ε_{Nd} were also successfully applied to infer the contribution of terrigenous sediments from the Mozambique Channel and in turn oceanic transport pathways around the tip of South Africa [*Franzese et al.*, 2006].

For this study, we analyzed the ε_{Nd} signatures of clay-sized fraction from sediment core 64PE304-80, which has been recovered ∼200 km north of the Zambezi mouth at ∼1329 m water depth, where a continuous deposition of fine-grained riverine-derived sediment has taken place over the past ∼45 kyr [*van der Lubbe et al.*, 2014]. Based on modern provenance and surface sediment distributions, the down-core ε_{Nd} signatures of the clay-sized fraction of core 64PE304-80 were used to reconstruct changes in climate-driven provenance and transport pathways of the lithogenic clay fraction along the Mozambique Margin.

2. Geography and Geology of the Zambezi Catchment

According to the position of the CAB and the ITCZ and the presence of mountain ranges, the annual precipitation displays a pronounced latitudinal gradient from >1000 mm in the northern part of the catchment to <500 mm in the south (Figures 1a, 2a, and 2b). The Zambezi originates in the humid Angolan highlands, which act as watershed between the Zambezi and Congo catchments. Downstream the Victoria Falls, the Zambezi flows through extensive floodplains, joined by several tributaries. The surface geology in this area is dominated by sandy soils belonging to the Cenozoic Kalahari Formation (Figure 2c). Further downstream, the Zambezi incises into the underlying sediments before finally plunging over the Victoria Falls [*Moore et al.*, 2008]. Prior to the establishment of the Victoria Falls that occurred ∼1.8 Ma ago, the upper Zambezi flowed westward, discharging into the South Atlantic Ocean [*Moore et al.*, 2008; *Walford et al.*, 2005]. The subsequent easterly flow of the Zambezi led to an increased catchment size, associated with increased sediment accumulation offshore the Zambezi mouth [*Walford et al.*, 2005]. The upper part of the Zambezi Catchment provides a third of the total Zambezi outflow, but its estimated sediment contribution (∼0.1 Mm^3) [*FFEM*, 2005] is negligible because of the low elevation gradients and the low degree of geochemical weathering (Figures 2a and 2b). In the lower part of the Zambezi Catchment, the dammed Lake Cahora Bassa receives ∼29 Mm^3 sediment per year [*FFEM*, 2005] (Figures 2a and 4). Most of the suspended sediments are probably delivered by the large Kafue and Luangwa Rivers that drain highland areas with intensely weathered, clayey soils and high precipitation exceeding >1000 mm/yr (Figure 2b). The remaining ∼22 Mm^3 of the total annual Zambezi sediment load (∼51 Mm^3) is derived from drainage areas downstream the Cahora Bassa dam [*FFEM*, 2005]. Most of the discharge originates from the Shire River that receives overflow from Lake Malawi [*Moore et al.*, 2008], which itself acts as a sediment trap providing important local climate records [e.g., *Castaneda et al.*, 2009; *Konecky et al.*, 2011].
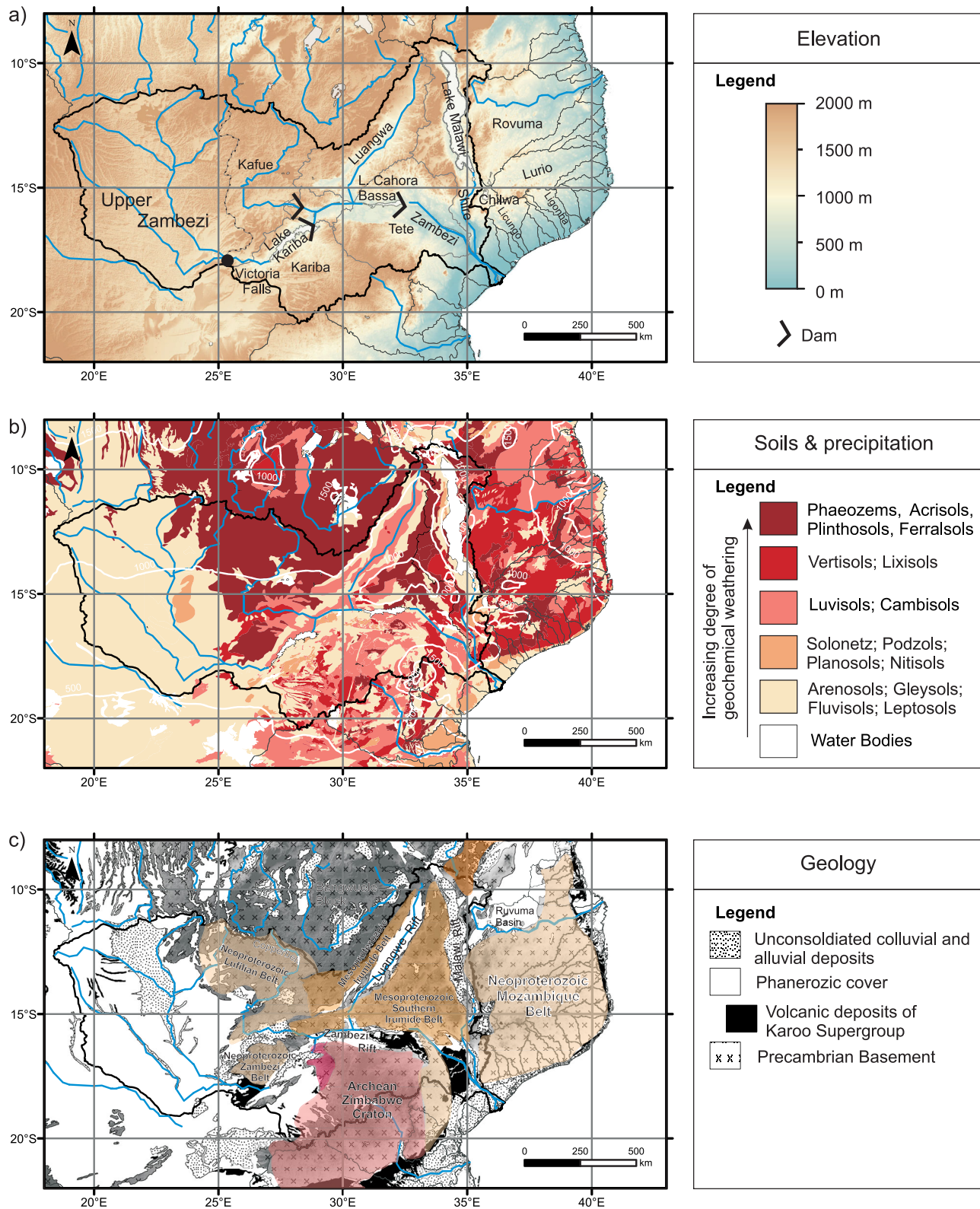
Figure 2.

Table 1. Selected Radiocarbon Ages

Lab ID	Core	AMS ^{14}C Age	(+/−)	cal. yr BP	(+/−)	Depth Scale of Core 64PE304-80 (cm)	cal. yr BP	Reference[a]
KIA 45243	64PE304-80	450	30/30	59	58/23	10	0	2
KIA 43167	GIK16160-3	3,970	30/30	3,967	62/53	101	3,973	1
KIA 43827	64PE304-80	6,145	35/35	6,579	50/54	188	6,542	2
KIA 43829	64PE304-80	7,940	40/40	8,400	45/38	223	8,380	2
KIA 41418	GIK16160-3	9,930	50/50	10,178	41/46	253	10,065	1
KIA 41419	GIK16160-3	10,560	60/60	11,797	120/154	283	11,771	1
KIA 41420	GIK16160-3	11,620	70/70	13,118	52/116	306	13,228	1
KIA 41421	GIK16160-3	13,070	70/70	14,984	184/196	358	14,799	1
KIA 41422	GIK16160-3	13,590	70/70	16,067	216/399	388	16,089	1
KIA 43168	GIK16160-3	14,270	70/70	15,834	319/420	424	16,897	1
KIA 45244	64PE304-80	15,400	70/70	18,253	196/87	488	18,401	2
KIA 45245	64PE304-80	16,360	80/80	19,135	183/149	515	19,211	2
KIA 41424	GIK16160-3	17,170	120/120	19,923	97/214	568	20,394	1
KIA 45246	64PE304-80	17,870	110/110	20,798	294/242	605	21,263	2
KIA 43821	64PE304-80	20,530	260/140	24,052	193/212	659	23,773	3
KIA 43169	GIK16160-3	23,750	190/190	26,485	240/196	781	28,540	1
KIA 43822	64PE304-80	26,210	260/270	30,619	236/251	834	30,627	3
KIA 43823	64PE304-80	28,360	320/340	32,182	544/408	875	32,898	3
KIA 45247	64PE304-80	30,200	360/370	34,402	405/443	935	34,647	3
KIA 43179	GIK16160-3	32,750	590/590	36,990	673/853	968	36,165	1
KIA 43824	64PE304-80	34,640	680/740	39,221	757/1,177	1,005	38,412	3
KIA 43825	64PE304-80	37,740	970/1,100	42,050	792/855	1,071	41,560	3

[a]References: 1, *Wang et al.* [2013]; 2, *van der Lubbe* [2014]; 3, S. Kasper et al. (submitted manuscript, 2014).

The Zambezi Catchment exhibits a wide range of rock types and geological formations (Figure 2c), which have markedly different radiogenic isotope signatures. The southern bank of the lower Zambezi is formed by the Archean Zimbabwe Craton, which has average ε_{Nd} values of ∼−29 [*Jelsma et al.*, 1996], whereas partial melting of an older source led to unradiogenic ε_{Nd} values of ∼−41 [*Grantham et al.*, 2011] (Figure 4). On the northern bank, the bedrock geology is dominated by the Mesoproterozoic Irumide Belt that is separated by the Luangwe Rift, which contains significantly younger deposits of the Jurassic Karoo Formation. Due to recycling of older crust and the addition of younger material, the ε_{Nd} values of the whole-rock samples of the southern Irumide Belt southwest of Lake Malawi cover a wide range roughly between −16 and −3 [*Kroner et al.*, 2001], while less radiogenic ε_{Nd} values between −20 and −15 are found in Irumide Belt north of the Luangwe Rift [*De Waele et al.*, 2006]. The most radiogenic ε_{Nd} values between −3 and −1 are represented by the young basalts of the Karoo Super-group [*Jourdan et al.*, 2007]. Before plunging over the Victoria Falls, the Zambezi starts to incise into the underlying sediments of the Kalahari Formation and Karoo Basalts [*Moore et al.*, 2008]. The unconsolidated sands of the Cenozoic Kalahari Formation have relatively radiogenic ε_{Nd} values of −5.2 to −3.8 as found in eolian deposits, which are present in a large area outside the Zambezi Catchment [*Grousset et al.*, 1992]. Due to the prevailing easterly winds and the absence of other large regional dust source areas, lithogenic sediments in the Mozambique Channel have a dominantly riverine origin and thus their properties must be directly related to continental hydrological conditions.

3. Offshore Dispersal of Zambezi Sediment

During peak discharge of the Zambezi following maximum austral summer precipitation, a large plume of suspended sediment extends from the Zambezi mouth to the northeast along the Mozambique coast and deposits as a narrow mud-belt [*Beiersdorf et al.*, 1980; *Schulz et al.*, 2011; *Siddorn et al.*, 2001]. With its annual sediment load of ∼51 Mm^3, the Zambezi is the largest single suspended sediment supplier to the

Figure 2. Maps of southeast Africa, with Figure 2a showing the topography with riverine catchments delineated by thin black lines, whereas the Zambezi Catchment is indicated by a thick black line. Subdrainages of the Zambezi and relatively large rivers draining the area east of Lake Malawi are labeled as well as natural and anthropogenic lakes. The N-S dashed line marks the eastern boundary of the upper part of the Zambezi Catchment, which discharges to the Victoria Falls. The major rivers are indicated by thick blue lines. The elevation and derived hydrological data are obtained from the HYDRO1k database. Figure 2b shows the soils types [*FAO/IIASA/ISRIC/ISS-CAS/ JRC*, 2009] that are ranked to their degree of weathering as well as contours of annual precipitation (mm) that are derived from the CRU database outlined in white color. Figure 2c represents a simplified geological map [*Geological Survey of Canada*, 1995] with the main tectonic-structural units [*Roberts et al.*, 2012] in southeastern Africa.
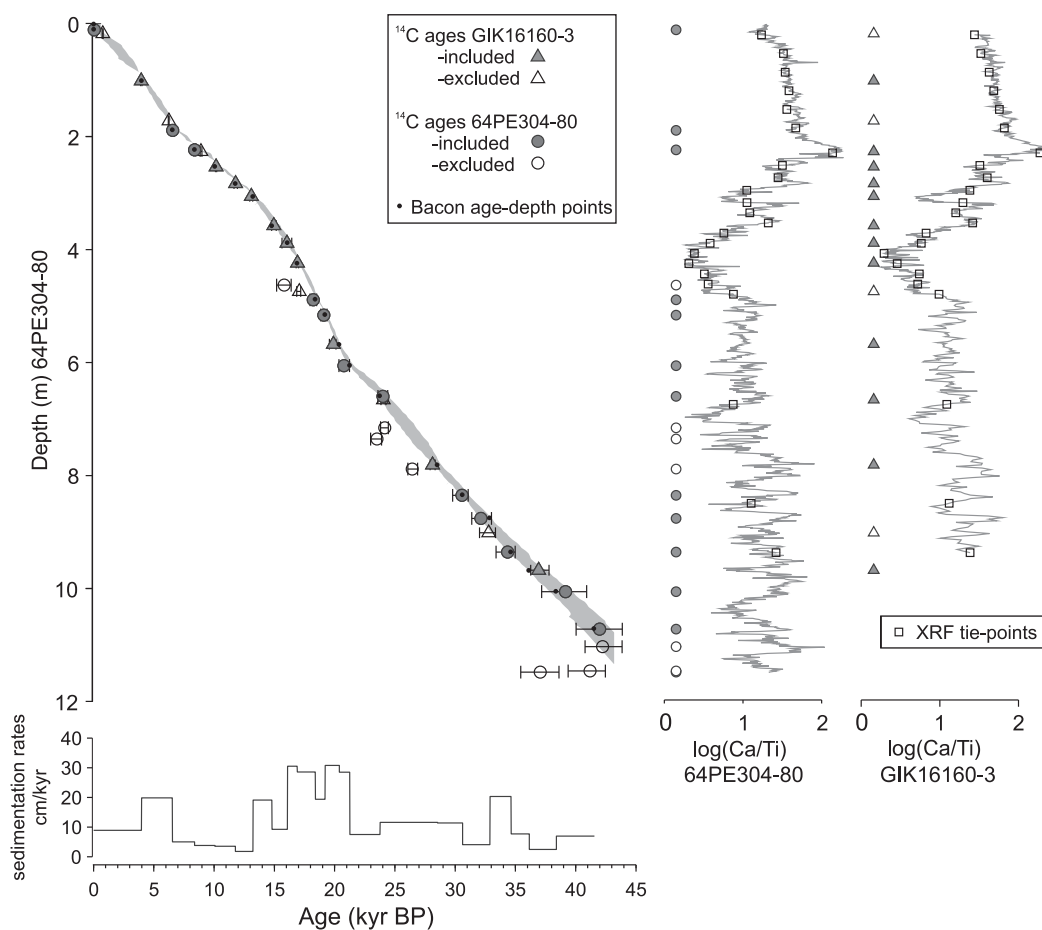
Figure 3. Age-depth model of core 64PE304-80. The left top figure shows the age-depth model of the core 64PE304-80 with 90% confidence limits that was constructed using age-depth modeling program BACON, whereas the bottom figure displays sedimentation rates inferred from the BACON age-depth points. The AMS ^{14}C ages were obtained for core 64PE304-80 as well as derived from parallel core GIK16160-3, which can be stratigraphically linked using the comparable log (Ca/Ti) records [van der Lubbe et al., 2014] (right).

Mozambique Margin [*Walford et al.*, 2005]. Most of the Zambezi suspension load is likely spilled over from the Mozambique Shelf at ∼18°S, where the mud-belt is situated close to the slope [*Schulz et al.*, 2011]. A large portion is then probably transported downslope by gravity currents through connecting submarine channels, and finally deposited on the large Mozambique deep-sea fan (Figure 1a), which is situated at the southern end of the Mozambique Channel [*Kolla et al.*, 1980a]. The outer shelf is covered by sands due to winnowing by oceanic, tidal, and wave-induced currents [*Beiersdorf et al.*, 1980]. Oceanographic observations also indicate a strong mean flow exceeding 40 cm/s in the surface waters, which is generated by large anticyclonic eddies that frequently propagate southward along the continental slope [*Ullgren et al.*, 2012]. High amounts of clay (>70%) are deposited on the slope at ∼500 m water depth at locations between the Zambezi mouth and ∼16°S in relatively calm water [*Schulz et al.*, 2011]. Re-suspension of sediments by bottom currents takes place along the slope [*Fallet et al.*, 2012] forming a dense nepheloid layer attributed to the high availability of fine-grained material in the Mozambique Channel [*Kolla et al.*, 1980b]. The southward flow is compensated by a northward flowing bottom current carrying Antarctic Intermediate Water (AAIW) and North Atlantic Deep Water (NADW) at water depths below 1500 m [*de Ruijter et al.*, 2002]. Due to the decreasing flow speeds, the hemipelagic deposition of fine-grained sediments increases below ∼1000 m water depth, in particular south of ∼18°S [*Schulz et al.*, 2011]. Depending on sinking rates and lateral advection by bottom currents, a considerable portion of the fine-grained sediments may originate from sources as far north as 10°S, where the Northeastern Madagascar Current (NEMC) splits when approaching the southeast African coast (Figure 1a).

During glacial and deglacial sea level lowstands, the Zambezi incised into the wide, subaerially exposed shelf, thereby discharging its sediments directly onto the upper slope [*Beiersdorf et al.*, 1980]. Flooding of the shelf and the Zambezi paleo-valley after the last deglacial sea level rise drastically reduced the accumulation of fine-grained sediment off the Zambezi mouth. On the contrary, the clay deposition increased in the north, since shelf flooding facilitated the NE transport of Zambezi sediments [*van der Lubbe et al.*, 2014].

Before interpreting down-core variations, the ε_{Nd} signature of the Zambezi suspension was determined based on surface sediment clays from the wide Mozambique Shelf, which are overwhelmingly derived from the Zambezi. In addition, the surface clays from the Mozambique slope further to the north were analyzed for their ε_{Nd} signatures in an attempt to identify more northerly situated sediment sources. Afterward, the ε_{Nd} variations of the clays of the past ∼45 kyr were compared to other lithogenic sediment properties (clay content and magnetic susceptibility) as well as previously published organic proxy records of soil-derived organic matter and precipitation [*Schefuss et al.*, 2011; *Wang et al.*, 2013; S. Kasper et al., delta Deuterium of alkenone and BIT index of sediment core 64PE304-80 samples, submitted to *Organic Geochemistry*, 2014], in order to disentangle the effects of sea level changes, oceanic currents, and Zambezi discharge on sediment deposition along the Mozambique Margin.

4. Material and Methods

4.1. Sediment Core and Samples

Piston core 64PE304-80 (18°14.44′S, 37°52.14′E) was recovered from 1329 m water depth during the INATEX cruise in 2009 with the research vessel RV Pelagia [*Brummer et al.*, 2009]. Core 64PE304-80 was chosen because it is located ∼200 km north of the Zambezi mouth, away from the Zambezi paleo-channel and shelf-break, and therefore less sensitive to shifts in local depocentres and sea level fluctuations than shallow cores from the Mozambique Margin. The core is characterized by continuous lithogenic sandy mud accumulation throughout the ∼11.5 m except a small turbidite interval centered on 69 cm core depth. Core 64PE304-80 was obtained near core GIK16160-3, which was retrieved with a gravity corer during METEOR cruise M75-3 in 2008 [*Schneider et al.*, 2008]. Shelf surface sediments were obtained from core tops retrieved during the M75-3 and INATEX cruises. Locations and water depths of the surface sampling sites are listed in Table 3. A sample of Zambezi sands was retrieved from ∼175 km upstream of the Victoria Falls Sesheke, Zambia.

4.2. Chronology

The chronology of core 64PE304-80 is based on previously published AMS ^{14}C determinations, obtained from mixtures of planktonic foraminiferal species (∼1 mg of *Globigerinoides ruber, Globigerinoides trilobus*, and *Globigerinoides sacculifer* from the fraction >150 μm) [*van der Lubbe et al.*, 2014; S. Kasper et al., submitted manuscript, 2014]. The chronology was improved by including an additional AMS ^{14}C determination (KIA 43179; Table 1) obtained by the Leibniz-Laboratory for Radiometric Dating and Isotope Research (Kiel, Germany) on a planktonic foraminifera sample. Further age constraints were obtained from neighboring core GIK16160-3 by correlating their almost identical log(Ca/Ti) records for the last 37 kyr [*van der Lubbe et al.*, 2014]. The ^{14}C raw data of the samples were converted to calibrated ages (cal. yr BP) using the Marine09 calibration curve [*Reimer et al.*, 2009] and a ΔR value of 0. The Marine09 calibration curve includes a built-in time-dependent global ocean reservoir correction of about −400 ^{14}C yr.

The Bayesian age-depth modeling program BACON [*Blaauw et al.*, 2011] was used to calibrate the ^{14}C AMS ages and to establish the age-depth model. The BACON age-depth model includes 90–95% confidence limits that were used to select reliable age samples (Table 1) and to exclude anomalies and age reversals. The BACON age-depth model of core 64PE304-80 reveals four intervals with age anomalies situated outside these age-depth confidence limits and a full age reversal below ∼10.7 m (Figure 3). Individual ^{14}C dates deviating from the reconstructed chronology using age-depth confidence limits, indicate ages of both cores that are too young for their stratigraphic depths, which is the result of the constructed age-depth model that avoids anomalous steps in overall sedimentation rates.

4.3. Sample Preparation

The lithogenic component of the clay-sized sediment fraction (<2 μm) was separated prior to analysis of the Nd isotope signatures. The clay fraction was isolated in settling tubes applying the Atterberg method

Table 2. Nd Isotope Ratios of the Detrital Clay Fraction in Core 64PE304-80

Depth in Core (cm)	εNd	+/−	Series
14.5	−15.1	0.2	2
55	−15.4	0.1	1
61.5	−15.4	0.1	3
65.5	−15.0	0.2	2
110	−15.2	0.2	1
143.5	−14.6	0.2	2
163.5	−14.0	0.1	3
170	−14.1	0.1	1
188.5	−14.1	0.3	2
219.5	−13.7	0.1	1
223.5	−13.4	0.1	3
233	−13.1	0.2	2
269.5	−13.1	0.2	1
273	−13.1	0.2	2
283.5	−14.4	0.1	3
298	−13.7	0.2	2
307.5	−13.5	0.2	2
310	−13.6	0.1	1
330	−13.6	0.1	1
332.5	−13.9	0.1	2
362.5	−14.1	0.2	2
380	−14.5	0.1	1
382.5	−14.7	0.1	2
410	−14.7	0.1	1
417.5	−14.6	0.2	2
462.5	−14.9	0.1	3
470	−14.5	0.1	1
485	−14.4	0.1	3
517.5	−14.2	0.2	2
559.5	−14.3	0.1	1
584	−14.4	0.1	3
640	−14.6	0.1	1
643.5	−14.8	0.1	3
735.5	−14.2	0.1	3
739.5	−14.4	0.2	1
758	−14.8	0.1	3
774.5	−14.6	0.2	1
790.5	−13.5	0.1	1
820	−14.1	0.1	1
860	−14.2	0.1	1
868.5	−13.9	0.1	3
902	−13.5	0.1	1
918.5	−13.9	0.1	3
949.5	−13.7	0.1	1
969.5	−14.0	0.2	1
979	−13.5	0.1	3
979.5	−13.4	0.1	1
1003.5	−13.8	0.2	1
1040	−13.8	0.1	1
1048.5	−14.0	0.1	3
1058.5	−13.7	0.1	3
1060	−14.0	0.2	1

following *NEN Standard 5753* [2006]. After oxidation of the organic matter with H_2O_2, the samples were sieved to separate the coarse-grained fraction, in order to recover foraminifera for further analyses. The fine-grained sediment fraction was kept in suspension with the aid of sodium pyrophosphate. Prior to Nd isotope analyses, the bulk sediment samples were decarbonated using 1 M acetic acid at room temperature (Series 1), whereas samples of the second batch were brought to 100°C in 0.1 M HCl and thereafter cooled down to room temperature (Series 2), which is a standard preparation method for grain-size analysis [*Konert and Vandenberghe*, 1997]. For Series 3, the bulk sediment samples were oxidized and decarbonated in a mixture of 6% H_2O_2 and 1 M acetic acid at room temperature prior to separation of the clay fraction as described in detail by *Stumpf* [2011]. The lithogenic clay fraction of Series 3 was isolated from the decarbonated sediment fraction using the centrifuge-based Atterberg method. Clay samples of Series 1–3 were obtained from core 64PE304-80 (Table 2), whereas Series 1 and 3 also include shelf and slope surface sediments (Table 3).

The treatment with diluted acetic acid and HCl will remove the carbonate fraction (including coccolith and foraminiferal shells) that is relatively poor in Nd anyhow, but may not quantitatively remove the authigenic Fe-Mn oxyhydroxide fraction, which contains Nd that is precipitated in equilibrium with dissolved Nd in seawater [*Chester and Hughes*, 1967; *Gutjahr et al.*, 2007]. Leaching experiments of the decarbonated marine sediments, in which the Fe-Mn oyxhydroxide fraction was completely extracted revealed a Nd loss of ∼15–20% due to the removal of authigenic fraction as well as some of the detrital material [*Gutjahr et al.*, 2007]. For these sediments, the estimated offsets between the decarbonated bulk material and detrital fraction are 0.2–0.3 ε_{Nd} units, which is similar as the analytical 2σ uncertainties of the measurements in this study (Tables 2 and 3). In the open Indian Ocean, where the concentration of seawater Nd is relatively low, the

ε_{Nd} values range roughly between −9 and −7 [*Bertram and Elderfield*, 1993]. Along continental margins, in particularly near large river mouths such as that of the Zambezi, the Nd concentration increases and the Nd isotope signatures will be biased toward detrital sediment fraction due to release of adsorbed Nd from mineral surfaces and partial dissolution of the particles [*Jeandel et al.*, 2007]. Moreover, increased Zambezi discharge will lead to an increased sediment supply, as well as release of dissolved Nd along the Mozambique Margin. The contribution of authigenic Nd from seawater is therefore expected to be of minor influence on the measured Nd isotope compositions of the clays and the interpretations of this study. This is confirmed by the indistinguishable Nd isotope results for the three different series of core 64P304-80 (Table 2 and Figure 5), which underwent slightly different preparation methods.

Table 3. Nd Isotope Ratios of the Detrital Clay Fraction in Surface Sediment Samples

Core	Latitude	Longitude	Water Depth (m)	εNd	+/−	Series
64PE304-47	−14.57530	41.32963	2804	−11.2	0.1	1
64PE304-68	−16.50285	40.02523	756	−15.2	0.2	1
64PE304-66	−16.53418	40.05458	1103	−15.1	0.2	1
64PE304-56	−16.85128	41.31943	2652	−14.4	0.1	1
GIK16158-2	−17.54950	37.96700	25	−16.6	0.2	3
GIK16159-1	−17.76317	37.92133	55	−16.4	0.2	3
GIK16160-1	−18.24133	37.86900	1343	−15.8[a]	0.2	3
GIK16157-4	−18.72217	36.54117	18	−17.7	0.1	3
64PE304-82	−18.87800	37.39998	939	−15.3	0.1	1
GIK16156-5	−18.93583	36.40283	24	−16.2	0.2	3
GIK16156-1	−18.94283	36.40967	n.a.	−16.5	0.1	3
64PE304-86	−19.35168	36.87368	197	−14.7	0.1	1
64PE304-88	−19.37030	36.90217	410	−15.7	0.2	1
GIK16155-1	−20.86533	35.89567	836	−16.1	0.2	3
Sands of Zambezi headwaters ∼175 km upstream the Victoria Falls (Sesheke, Zambia)				−6.0	0.1	3

[a]Average of two measurements.

4.4. Nd Isotope Analysis

About 20 mg of homogenized and powdered material of the clay fraction was completely dissolved using a mixture of conc. HF-HNO_3-$HClO_4$. Subsequently, Nd was purified applying standard ion chromatographic procedures [e.g., *Stumpf*, 2011]. The international marine mud standard MAG-1 was repeatedly run through the analytical procedures as a reference. The Nd isotopic measurements of samples of Series 1 were performed at the Vrije Universiteit (Amsterdam) using a MAT-262 Thermal Ionization Mass Spectrometer (TIMS). Blanks typically yielded <300 pg, which has a negligible effect on the measured isotope ratios. The accuracy and precision of the TIMS Nd isotope measurements was monitored by repeatedly analyzing the in-house CIGO standard that gave an average $^{143}Nd/^{144}Nd$ value 0.511345 ± 0.000007 (2σ; n = 4), which is consistent to the long-term average 0.511332 ± 0.000011 (2σ; n = 123). The international standard MAG-1 that was repeatedly run through the entire total dissolution procedures for each series gave a mean $^{143}Nd/^{144}Nd$ value of 0.512074 ± 0.000004 (2σ; n = 3), which is, within error, identical to the average value of 0.512070 ± 0.000012 that had been measured at the Vrije Universiteit Amsterdam before, as reported by *Meyer et al.* [2011]. The radiogenic $^{143}Nd/^{144}Nd$ ratios of the samples are reported as ε_{Nd} values, which correspond to the deviations of the $^{143}Nd/^{144}Nd$ values of the samples that from the present-day Chondritic Uniform Reservoir (CHUR) value of 0.512638 [*Jacobsen et al.*, 1980]. Sample Series 2 and 3 were analyzed for their Nd isotope signatures on a Nu Instruments multicollector inductively coupled plasma mass spectrometer (MC-ICP-MS) at GEOMAR, Kiel. The $^{143}Nd/^{144}Nd$ ratios were mass bias corrected to $^{146}Nd/^{144}Nd = 0.7219$ and were then normalized to the accepted value of the JNdi-1 standard of 0.512115 [*Tanaka et al.*, 2000].

4.5. Magnetic Susceptibility, Clay Content, and Bulk Chemistry

Bulk low field magnetic susceptibility (MS) was measured every centimetre for split sediment core 64PE304-80 using a GEOTEK Multi-Sensor Core Logger equipped with a Bartington surface magnetic susceptibility point sensor (MS2E) at Department of Earth Sciences, Vrije Universiteit (Amsterdam). Sediment samples that were taken every 5 cm in core 64PE304-80 had previously been analyzed for lithogenic grain-size distributions using a Sympatec HELOS/KR laser diffraction particle size analyzer at the Laboratory for Sediment Analysis, the Vrije Universiteit (Amsterdam) [*van der Lubbe et al.*, 2014]. Lithogenic grain-size distribution and magnetic susceptibility records of the upper part of core 64PE304-80 were previously published by *van der Lubbe et al.* [2014]. The grain-size distributions measured by laser diffraction overestimate the particle size of the clay fraction separated by settling due to the platy structure of clay minerals [*Konert and Vandenberghe*, 1997]. The down-core variations in the clay size fraction (<2 μm) that was separated for Nd isotope analysis were thus estimated using the <8 μm lithogenic fraction measured by the laser particle sizer (Figure 5e). The C/N ratios of the parallel core GIK16160-3 were determined for this study using duplicate samples from every 10 cm, based on ∼10 mg of freeze-dried sediment powder using a CARLO ERBA Elemental Analyser at GEOMAR (Kiel, Germany).
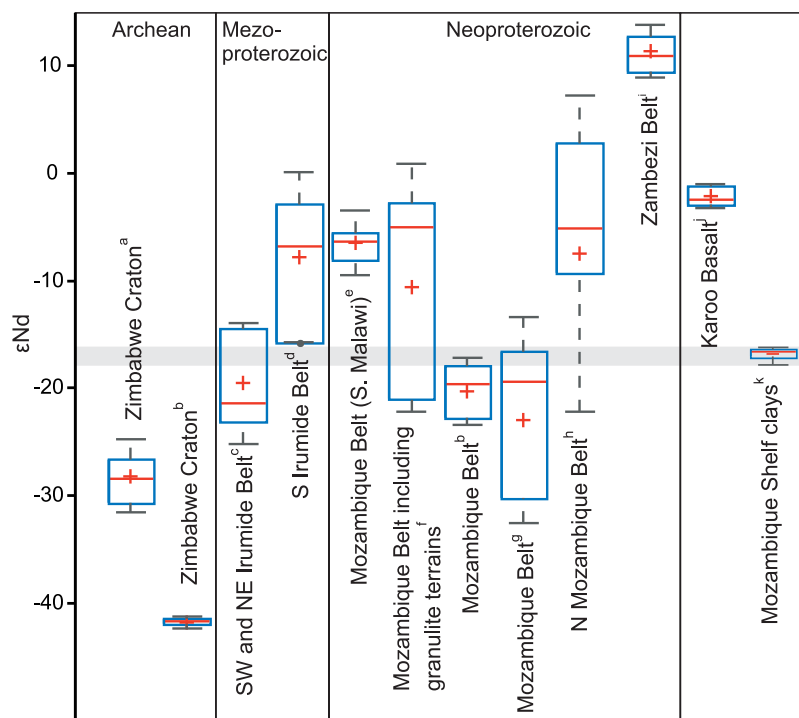
Figure 4. Comparison of ε_{Nd} values obtained from surface clays of the Mozambique Shelf with ε_{Nd} values of whole-rocks samples of potential source rocks using box and whisker plots with mean and median indicated by crosses and horizontal red lines, respectively. References: [a]Jelsma et al., [1996], [b]Grantham et al., [2011], [c]De Waele et al., [2006], [d]Johnson et al., [2007], [e]Kröner et al., [2001], [f]Möller et al., [1998], [g]Vogt et al., [2006], [h]Hauzenberger et al., [2007], [i]John et al., [2004], [j]Jourdan et al., [2007] and [k]This study.

5. Results

5.1. Nd Isotope Signatures of Surface Sediments

Relatively unradiogenic ε_{Nd} values between −17.7 and −16.2 are found in surface sediment clays from the wide Mozambique Shelf, which directly receives discharge from the Zambezi River (Table 3 and Figure 1b). Clays that were extracted from the adjacent continental slope yield somewhat more radiogenic ε_{Nd} values of −15.8 to −14.7. Even more radiogenic values of −14.4 and −11.2 are found for detrital clays in the central Mozambique Channel at ∼17°S and ∼2700 m water depth and from the continental slope at ∼15°S and ∼2800 m water depth, respectively. The most radiogenic ε_{Nd} value of −6 was measured for sands that were collected from the Zambezi headwaters, upstream from the Victoria Falls.

5.2. Sediment Core 64PE304-80
5.2.1. Magnetic Susceptibility and Clay Content

On average, ∼35% of the lithogenic sediments is within the clay-sized fraction. The down-core clay content shows distinct variations over the past ∼45 kyr, which closely resemble changes in the ε_{Nd} record. Relatively low amounts of clay (<30%) are found during Marine Isotope Stage (MIS) 3, whereas percentages above 30% occurred during MIS 2 reaching highest values during Heinrich Stadial (HS) 1 (Figure 5e). Similar amounts were deposited during the Younger Dryas (YD) and thereafter decreased again to ∼30% during the early Holocene. At ∼9 ka, the clay content started to increase and reached maximum values during the past ∼6 kyr. The variations in clay content parallel the MS record, whereby relatively low clay contents correspond to high MS values (Figure 5d). As a consequence, the magnetic susceptibility record displays high values during the latest MIS 3, which are subsequently reduced during MIS 2. At ∼15 ka the magnetic susceptibility sharply increased, developing a distinct double peak, which is a feature common in sediment cores from the Mozambique Margin [*Just et al.*, 2014; *März et al.*, 2008; *Schulz et al.*, 2011]. Relatively low MS values within this double peak coincide with the YD interval. Around 9 ka, the MS record drops to consistently low values, which increased slightly during the last ∼2 kyr. The MS record reflects iron oxides that have a detrital origin related to erosion [*Just et al.*, 2014] and are associated with relatively coarse-grained
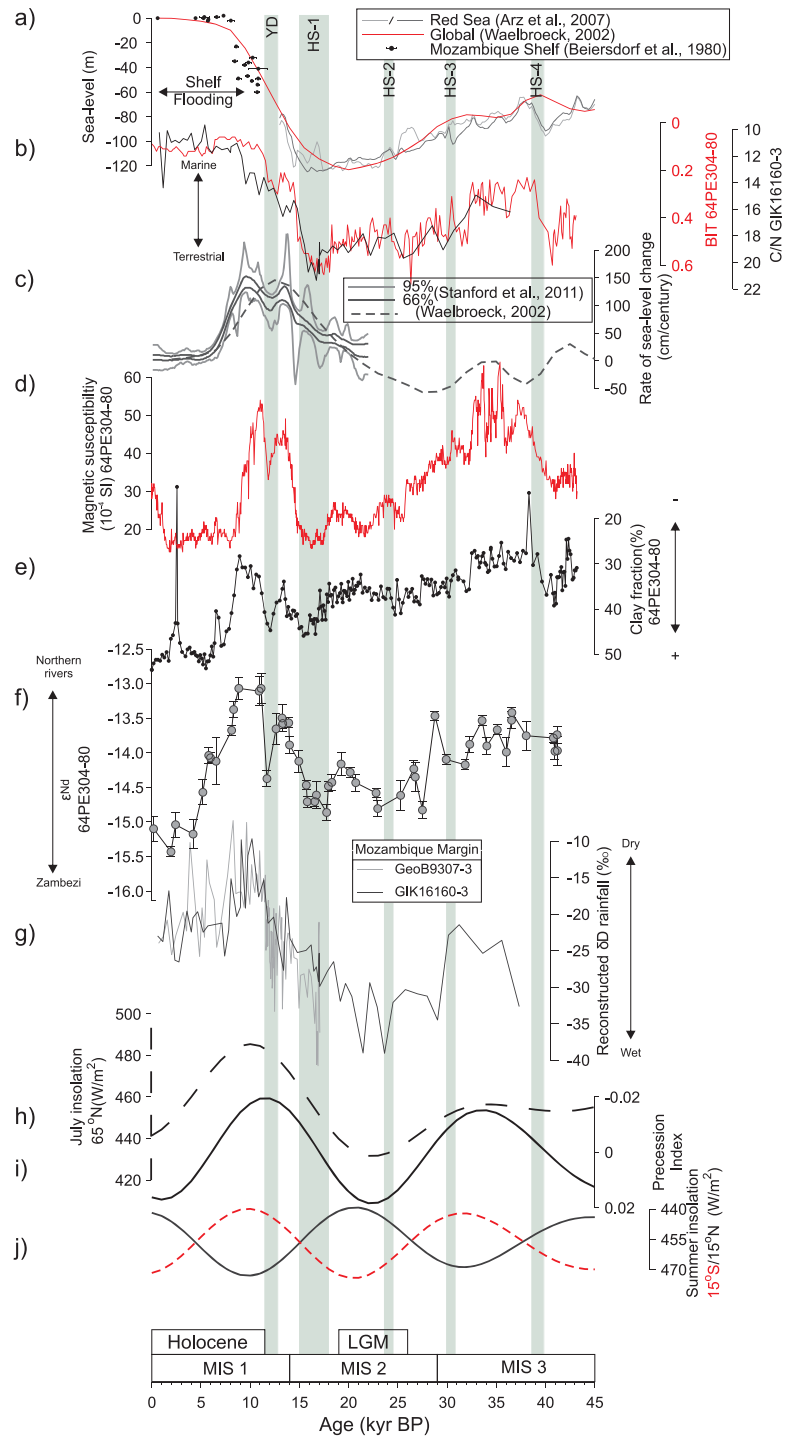
Figure 5. Lithogenic proxy records of core 64PE304-80 in combination to organic proxy records of this core and parallel core GIK16160-3. (a) Global and Red-Sea sea level curves with flooding history of Mozambique Shelf. (b) C/N ratios of core GIK16160-3 and BIT (S. Kasper et al., submitted manuscript, 2014) record of core 64PE304-80 reflect the relative contribution of soil organic matter input. (c) Rate of sea level change from *Stanford et al.* [2011] and deduced from the global sea level curve of *Waelbroeck* [2002]. (d) Magnetic susceptibility, (e) clay content, and (f) ε$_{Nd}$ signatures of the clay fraction document changes in sediment provenances in core 64PE304-80. (g) Reconstructed δD precipitation based on leaf wax (n-C31 alkanes) corrected for C$_3$/C$_4$ abundances following *Collins et al.* [2013] and ice-volume for cores GIK16160-3 [*Wang et al.*, 2013] and GeoB9307-3 [*Schefuss et al.*, 2011]. Records of (h) July 65°N insolation, (i) the precession index, and (j) summer insolation at 15°N and 15°S [*Laskar et al.*, 2004]. The Younger Dryas (YD) and Heinrich stadials HS-1 to HS-4 are indicated by vertical gray bars.

sediments transported downslope [*Schulz et al.*, 2011]. The observed variations in MS can be therefore mainly explained by dilution by the fine-grained lithogenic input. The carbonate and organic matter content of parallel core GIK16160-3 is generally low and averages ∼20 and ∼1%, respectively [*van der Lubbe et al.*, 2014]. The C/N ratio of core GIK16160-3 reflecting the ratio between marine and terrestrial-derived organic matter matches the record of the BIT that was previously obtained from core 64PE304-80 (S. Kasper, submitted manuscript, 2014) (Figure 5b).

5.2.2. Nd Isotope Record of Detrital Clay

The high-resolution detrital clay ε_{Nd} record from core 64PE304-80 was established on a total of 52 clay samples (Table 2 and Figure 5f) and can be divided into distinct intervals. During MIS 3, the ε_{Nd} values range from −14.2 and −13.4, whereas slightly less radiogenic ε_{Nd} values dominated during MIS 2 with consistently lower ε_{Nd} values (between −15.0 and −14.5) during the period corresponding to HS-1. From ∼15 ka onward, the ε_{Nd} values increase and reach maximum values of up to −13.1 between 11 and 9 ka. A relatively low ε_{Nd} value of ∼−14.4 is found in clays deposited during the YD. From 9 ka to the present, ε_{Nd} values became systematically less radiogenic. The least radiogenic ε_{Nd} values are found from ∼5 ka onward, which are comparable to surface sediments from the Mozambique slope, offshore the Zambezi mouth.

6. Discussion

6.1. Potential Source Areas of Sediments of the Mozambique Margin

Considering the high discharge rates of the Zambezi and the dominant northeast directed sediment dispersal, the ε_{Nd} values of surface clays from the Mozambique Shelf are considered characteristic for the Zambezi suspension load. An ε_{Nd} clay value of −17.7 is obtained from surface sediments of the mud-belt in front of the modern active, northern branch of the Zambezi. Due to recent damming of the Zambezi River, this sediment sample may be somewhat biased to the source area downstream of Lake Cahora Bassa (Figure 2). Averaging of the ε_{Nd} shelf surface clay values provides a robust ε_{Nd} mean value of −16.7 (1σ ± 0.6, n = 5), which can be considered as representative for the Zambezi suspension load. This ε_{Nd} value is in good agreement with previous estimates for the ε_{Nd} signature of Zambezi Catchment sediments (Figure 2) [*Jeandel et al.*, 2007].

The radiogenic ε_{Nd} value of ∼−6 measured for Zambezi sands upstream of the Victoria Falls is in agreement with previously reported values of the Kalahari sands [*Grousset et al.*, 1992]. This unradiogenic ε_{Nd} values suggest that these sands might be locally derived from the underlying basalt of the Karoo Formation. U-Pb zircon ages indicate that sediments upstream the Victoria Falls are usually derived from eastern Neoproterozoic Lufilian Belt with smaller inputs from the Mezoproterozoic Kibaran and Irumide Belts [*Gärtner et al.*, 2014]. However, the sediment transport across the Victoria Falls is nowadays negligible compared to sediment contributions further downstream and is therefore too small to affect the clay ε_{Nd} signatures further downstream.

Due to transport and mixing in the lower part of the Zambezi Catchment, the clay ε_{Nd} signatures show a narrower range than the ε_{Nd} values of whole-rock samples of potential source terrains. As is shown in Figure 4, the ε_{Nd} values plot between the signatures of the most contrasting bedrock geologies in the catchment area, namely rocks of the old Archean Zimbabwe Craton and young basalts of the Karoo Formation. The ε_{Nd} signatures of the clays overlap with ranges of diverse bedrock lithologies of the Mezo- and Neoproterozoic orogenic belts. Fine-grained sediments derived from various bedrock geologies are transported and mixed over large distances and therefore a providing an ε_{Nd} signature integrated over the Zambezi Catchment. For this reason, it is also difficult to resolve the precise sediment source areas for detrital clay fraction using ε_{Nd} values only. Based on U-Pb ages of individual zircons, the Mezo- and Neoproterozoic orogenic belts have been previously identified as the main sediment source areas of Zambezi together with only minor contributions from the Archean to Paleoproterozoic terrains [*Iizuka et al.*, 2013]. The Mezo- and Neoproterozoic orogenic belts are situated in the northern part of the Zambezi Catchment, where the annual precipitation is highest due to high elevation and the northerly position of the ITCZ-induced rainfall belt. These areas are subject to intense chemical weathering and are most likely the main source of the Zambezi suspension load.

Once Zambezi sediments are discharged onto the Mozambique Shelf, they are transported across the shelf to the slope under the influence of eddy-induced oceanic currents. Surface sediments from the deep-sea Mozambique Channel have more radiogenic ε_{Nd} values than those obtained from the adjacent slope, whereas most radiogenic ε_{Nd} values have been found in the Mozambique Channel in the North. This offset indicates that Zambezi sediments are mixed to some extent with clays characterized by more radiogenic ε_{Nd} signatures from the north (Figure 1b). Given the dominantly southward surface circulation, discharges from other rivers such as the relatively large Lurio and Rovuma Rivers (Figure 2a) that drain the humid highlands east of Lake Malawi are likely to contribute material to coring site 64PE304-80 originating from as far north as ~10°S, where the NEMC splits as it approaches the African coast (Figure 1a). The bedrock of these drainage areas is mainly formed by the Neoproterozoic Mozambique Belt covered by geologically younger volcanic and sedimentary deposits in the coastal zone (Figure 2c). Due to the strong and turbulent eddy-induced currents, hemipelagic muds deposited along the Mozambique Margin may even partly originate from the volcanic lineament of the Comoros Archipelago and from rivers of NW Madagascar, which drain considerable portions of geologically younger formations. This interpretation is supported by Lagrangian back trajectories of foraminifera deposited along the Mozambique slope, which even have higher sinking rates than clay minerals [*Steinhardt et al.*, 2014; *van Sebille et al.*, 2015]. The southward sediment transport is also recorded by radiogenic isotope signatures of the detrital fraction typical for a Mozambique Channel origin all the way down into the Agulhas Current system [*Franzese et al.*, 2006].

6.2. Clay Deposition and Provenance Changes Over the Past ~45 kyr

Lithogenic grain-size analysis of sediment cores spanning a depth transect across the Mozambique Margin reveals that the clay accumulation rates are strongly affected by sea level rise during the last deglacial period [*van der Lubbe et al.*, 2014]. Prior to ~11 ka, the Mozambique Shelf was subaerially exposed and the Zambezi ran through a pre-existing paleo-valley [*Beiersdorf et al.*, 1980] (Figure 5a). During glacial and deglacial eustatic sea level minima, Zambezi clays were more dominantly transported by gravity currents from the Zambezi paleo-valley via connecting submarine canyons [*Kolla et al.*, 1980a]. The distribution of Zambezi sediments was mainly affected by oceanic surface currents on the upper slope until the wide, flat-lying part of the adjacent Mozambique Shelf started to flood and the Zambezi paleo-valley route became abandoned after the last deglacial sea level rise (Figure 5a). The postglacial increased transport distance of terrigenous material from the Zambezi mouth is reflected by organic properties, C/N ratio and BIT index (S. Kasper, submitted manuscript, 2014), which reach consistently high, marine-influenced values in upper-slope sediments after flooding of the shelf (Figure 5b). The complete flooding of the wide, shallow shelf facilitated the enhanced northeastward dispersal of Zambezi sediments as is attributed by an increased deposition of less radiogenic clays at coring site 64PE304-80/GIK16160-3 after ~5 ka BP. The lithogenic sediment properties (MS, clay content, and ε_{Nd} clay values) do not follow the same trend as the C/N ratio and BIT index, indicating that the Zambezi clay deposition was not primarily controlled by shelf flooding.

The rate of sea level fluctuation may have been also important shaping lithogenic sedimentary records at the continental slope, especially in case of rapid sea level fluctuations triggering remobilization and down-slope transport of sediment (Figure 5c). The interval that is characterized by the highest rates of sea level change coincides with relatively low clay content and high MS values as well as radiogenic ε_{Nd} values in core 64PE304-80. Considering the low river gradients and sediment trapping in the extensive floodplain areas upstream the Victoria Falls, it is not expected that an increased and/or seasonally varying rainfall amounts would have led to the enhanced deposition of more radiogenic sediments off the Zambezi mouth. In contrast, a more southward position of the African rainfall belt may have led to enhanced weathering, as well as contributions of sediments with relatively unradiogenic ε_{Nd} signatures derived from the Archean Zimbabwe Craton (Figure 2c). Given the strong N-S annual rainfall gradient over the Zambezi Catchment, the Zambezi suspension load is probably dominantly derived from the northern highlands in the lower part of Zambezi Catchment, where the rainfall is highest. The relatively unradiogenic ε_{Nd} value determined for the current Zambezi suspension load is therefore expected to be remain relatively constant over time. The most radiogenic ε_{Nd} values that occurred during the highest rates of sea level rise point therefore to relatively low contributions of Zambezi sediments and in turn low input from the adjacent slope. The high magnetic mineral and low clay contents, therefore rather reflect changes in the supply of Zambezi sediments to the coring site 64PE304-80 than sea-level-driven changes in clay transport and deposition.

In combination with the current ε_{Nd} distribution in surface clays, we propose a simple scenario to explain the ε_{Nd} variations for the past ∼45 ka BP by a two end-member mixing model of (1) relatively unradiogenic Zambezi sediments and (2) more radiogenic sediments from northerly riverine sources carried by the net southward flow of surface currents. Relative variations in deposition of Zambezi clays can be caused by changes in Zambezi discharge intensity, as well as changes in oceanic currents. Today, the net southward flow is induced by large anticyclonic eddies, which occasionally reach the bottom of the Mozambique Channel and can be therefore responsible for the reworking and dispersal of the fine-grained sediment fractions. For settling, clay minerals need to flocculate and prior to that can be transported over long distances. Once clays are deposited at the seafloor, they are relatively resistant to winnowing by oceanic currents due to cohesion. Variations in oceanic currents along the Mozambique Margin may explain the down-core changes in ε_{Nd} signatures of the clays. Relatively unradiogenic ε_{Nd} values coinciding with high abundances of clays and low MS might reflect reduced southward transport and in turn an increased deposition of riverine sediments close to their river mouths. The southward flow through the Mozambique Channel might be reduced when the ITCZ and consequently the SEC, which is situated in between wind-driven northern tropical and southern subtropical gyres, both shifted southward. A more southerly position of the SEC and bifurcation point of the NEMC may have reduced the southward flow through the Mozambique Channel. Up to now, however no proxy records have been available allowing for the reconstruction of changes in the current speed through the Mozambique Channel, but terrestrial vegetation and rainfall records have been established for sediment cores from the Mozambique Channel. Together with clay minerals, leaf waxes are deposited at the seafloor, which are also eroded from soils and transported by rivers. Carbon isotope composition ($\delta^{13}C$) in these leaf wax documents the relatively abundances between C_3- (shrubs and trees) and C_4-type (grasses) of vegetation, whereas the hydrogen isotope (δD) composition in leaf waxes reflects the δD precipitation, which is related to monsoon rainfall intensities over the Zambezi Catchment [*Schefuss et al.*, 2011; *Wang et al.*, 2013]. For the Mozambique Margin, δD-$\delta^{13}C$ leaf wax records have been established for two coring sites at the Mozambique Margin GIK16160-3/64PE304-80 and GeoB9307-3, of which the latter is located off the Zambezi mouth at 542 m water depth [*Schefuss et al.*, 2011; *Wang et al.*, 2013]. Offsets between the leaf wax isotope records suggest provenance differences between these coring sites. However, after correction for the contribution of C_3- and C_4-type vegetation, the deduced δD rainfall records are remarkably similar, despite their difference in sample resolution and the uncertainties in chronological control, and therefore provide a robust δD record of precipitation integrated over the region (Figure 5g). The similarity of the temporal pattern between the ε_{Nd} clay values and the two δD reconstructed precipitation records suggest that the ε_{Nd} record of the clays predominantly reflects Zambezi discharge intensities and, in turn, precipitation over the Zambezi Catchment. Consequently, more radiogenic ε_{Nd} signatures will reflect a considerable hemipelagic sediment deposition originating from northerly sources, i.e., when the Zambezi Catchment experienced drier conditions, while less radiogenic signatures document periods of higher rainfall intensity in this region and enhanced Zambezi discharge. Hence, the ε_{Nd} record documents relative contributions from different sources related to the variability of the African summer monsoon over the last ∼45 ka. Applying the relatively radiogenic ε_{Nd} values of the surface sediment clay particles in the north and those determined for the Zambezi as mixing end-members, the ε_{Nd} variations reflect a range of 40–80% contributions from the Zambezi catchment assuming comparable Nd concentrations for both end-members.

6.3. Paleo-climatological Implications

As discussed above, the ε_{Nd} clay record can be interpreted to reflect mainly changes in Zambezi discharge. The down-core record thus implies that discharge was lower during MIS 3 compared to MIS 2 and in particular to the Last Glacial Maximum (LGM) and HS-1. Thereafter, the Zambezi influence was further reduced reaching a minimum ∼11–9 ka, but the YD stands out as a recurrence period to wetter conditions in the Zambezi Catchment. After ∼9 ka BP, the Zambezi increasingly became the dominant clay source with highest contributions during the past ∼5000 years. The reconstructed Zambezi discharge shows an anti-phase relationship to Al/K ratios of the lithogenic fraction in marine sediment core GeoB1008-3, which reflects variations in degree of chemical weathering and Congo discharge and in turn precipitation integrated over a considerable part over northwest Africa [*Schneider et al.*, 1997]. Similar to the δD leaf wax record of Lake Tanganyika that is situated in the Congo Catchment, relatively wet conditions correspond to maxima in northern hemisphere summer insolation [*Tierney et al.*, 2010].

During reduced summer insolation at 65°N (Fig. 5h), the thermal gradient in the northern hemisphere was enhanced due to ice sheet expansion, which is expected to result in a more southerly position of the African precipitation belt and in turn wetter conditions over the Zambezi Catchment. In addition, the intervals of relatively low Zambezi discharge seem to be related to low precession indices of the Earth's orbit, leading to reduced summer insolation in the southern hemisphere (Fig. 5i-j). Such a concurrence is in agreement with another rare continuous sedimentary sequence in southeast Africa, namely from Lake Tswaing, which documented arid intervals linked to precession-related (19-23 kyr) minima in austral summer insolation [*Partridge et al.*, 1997]. The lowest Zambezi discharge is recorded between ∼15 and ∼7 ka ago, during the African Humid Period as inferred from northern hemisphere records [e.g. *Tjallingii et al.*, 2008] and coincides with low precession indices. The anti-phase relationship can be explained by a precession-related increase in southern hemisphere summer insolation (December–February) contrasting with decreased northern hemisphere summer insolation (June-August) (Fig. 5j). Opposite to the North [*Rossignol-Strick*, 1985], the latter might lead to an intensification of the precipitation belts at their southernmost extent due to an increased trans-equatorial air-pressure difference, land-sea temperature gradient, and in turn moisture transport. In contrast, the δD leaf wax record of Lake Malawi remained relatively stable during MIS 3 and 2 compared to the Holocene that is characterized by relatively δD enriched values supporting significant changes in precipitation, probably related to a shift in moisture source areas and pathways [*Konecky et al.*, 2011]. Unlike marine records, terrestrial records are more strongly affected by local precipitation effects related to the surrounding orography. This is clearly illustrated by the relatively wet conditions that are inferred for the YD and LGM from the sedimentary record of the small crater Lake Masoko, which is located in the northern part of the Lake Malawi drainage [*Garcin et al.*, 2006]. Consistent with these reconstructions, the ε_{Nd} clay record indicates relatively wet conditions in the Zambezi Catchment during YD and LGM (Figure 5f). Increased Zambezi discharge is expected a result of a seasonal southward shift of the ITCZ and CAB. To the opposite, the high-resolution δD leaf wax record of Lake Tanganyika shows distinct arid events at shorter time scale, which are considered to be time-synchronous to the northern hemisphere Heinrich stadials [*Tierney et al.*, 2010]. Northern hemisphere cooling and freshening of the North Atlantic Ocean during these Heinrich stadials is expected to shift the major atmospheric boundaries to the south causing wet/dry conditions in southern/northern Africa. Heinrich stadials earlier than HS-1 are not resolved in the ε_{Nd} record of core 64PE304-80, which is probably attributed to the relatively low resolution of the ε_{Nd} clay record prior to ∼20 ka BP as well as to their weaker expression in the tropics. Future higher-resolution climate proxy records from coring site 64PE304-80, which has sensitively documented variations of the Zambezi discharge have a large potential to even resolve more abrupt, centennial to millennial time scale variations as have been documented in SE Africa [e.g., *Brown et al.*, 2007; *Ziegler et al.*, 2013].

7. Conclusions

The Zambezi suspension load that is most likely derived from the highlands in the lower part of the catchment, where precipitation and geochemical weathering are highest due to the northerly position of the ITCZ has an averaged ε_{Nd} value of ∼17.6. On the adjacent continental slope, Zambezi sediments are mixed with more radiogenic clays, which are probably hemipelagic muds transported from more northerly sources under the influence of the eddy-induced net southward flow through the Mozambique Channel. The ε_{Nd} variation of clays in core 64PE304-80 that is situated just north of the Zambezi mouth reflects changes in the relative contribution of Zambezi sediments that have been linked to the δD changes in regional precipitation as are derived from δD leaf wax records [*Schefuss et al.*, 2011; *Wang et al.*, 2013]. Compared to the late MIS 3, MIS 2 was relatively wet with highest Zambezi runoff and contributions of riverine clays during the LGM and HS-1. Low Zambezi discharge is documented between ∼15 and 7 ka, which is contemporaneous with the African Humid Period recorded in North African paleoclimate records. Relatively wet conditions occurred during the YD and the late Holocene reaching modern levels ∼5 ka. The reconstructed sediment discharge of the Zambezi reflecting monsoonal precipitation variability followed precessional summer insolation over the last ∼45 kyr, which is in antiphase with the hydrological conditions from the northern Africa.

References

Bayon, G., B. Dennielou, J. Etoubleau, E. Ponzevera, S. Toucanne, and S. Bermell (2012), Intensifying weathering and land use in Iron Age Central Africa, *Science*, *335*(6073), 1219–1222, doi:10.1126/science.1215400.

Beiersdorf, H., H. R. Kudrass, and U. von Stackelbert (1980), *Placer Deposits of Ilmenite and Zircon on the Zambezi Shelf*, Schweizerbart, Stuttgart, Germany.

Bertram, C. J., and H. Elderfield (1993), The geochemical balance of the rare earth elements and neodymium isotopes in the oceans, *Geochim. Cosmochim. Acta*, *57*(9), 1957–1986, doi:10.1016/0016-7037(93)90087-D.

Blaauw, M., and J. A. Christen (2011), Flexible paleoclimate age-depth models using an autoregressive gamma process, *Bayesian Analysis*, *6*(3), 457–474.

Blanchet, C. L., R. Tjallingii, M. Frank, J. Lorenzen, A. Reitz, K. Brown, T. Feseler, and W. Brueckmann (2013), High- and low-latitude forcing of the Nile River regime during the Holocene inferred from laminated sediments of the Nile deep-sea fan, *Earth Planet. Sci. Lett.*, *364*, 98–110, doi:10.1016/j.epsl.2013.01.009.

Blanchet, C. L., M. Frank, and S. Schouten (2014), Asynchronous changes in vegetation, runoff and erosion in the Nile River Watershed during the Holocene, *Plos One*, *9*(12), 105–106, doi:10.1371/journal.pone.0115958.

Brown, E. T., T. C. Johnson, C. A. Scholz, A. S. Cohen, and J. W. King (2007), Abrupt change in tropical African climate linked to the bipolar seesaw over the past 55,000 years, *Geophys. Res. Lett.*, *34*, L20702, doi:10.1029/2007GL031240.

Brummer, G.-J. A., and S. Jung (2009), INATEX-GEO SE African margin, Rep., NIOZ, Royal Netherlands Institute for Sea Research, Netherlands.

Castaneda, I. S., J. P. Werne, T. C. Johnson, and T. R. Filley (2009), Late Quaternary vegetation history of southeast Africa: The molecular isotopic record from Lake Malawi, *Palaeogeogr. Palaeoclimatol. Palaeoecol.*, *275*(1–4), 100–112, doi:10.1016/j.palaeo.2009.02.008.

Chester, R., and M. Hughes (1967), A chemical technique for the separation of ferro-manganese minerals, carbonate minerals and adsorbed trace elements from pelagic sediments, *Chem. Geol.*, *2*, 249–262.

Collins, J. A., E. Schefuss, S. Mulitza, M. Prange, M. Werner, T. Tharammal, A. Paul, and G. Wefer (2013), Estimating the hydrogen isotopic composition of past precipitation using leaf-waxes from western Africa, *Quat. Sci. Rev.*, *65*, 88–101, doi:10.1016/j.quascirev.2013.01.007.

de Ruijter, W. P. M., H. Ridderinkhof, J. R. E. Lutjeharms, M. W. Schouten, and C. Veth (2002), Observations of the flow in the Mozambique Channel, *Geophys. Res. Lett.*, *29*(10), 1502, doi:10.1029/2001GL013714.

De Waele, B., J.-P. Liégeois, A. A. Nemchin, and F. Tembo (2006), Isotopic and geochemical evidence of Proterozoic episodic crustal reworking within the irumide belt of south-central Africa, the southern metacratonic boundary of an Archaean Bangweulu Craton, *Precambrian Res.*, *148*(3), 225–256.

Fallet, U., I. S. Castañeda, A. Henry-Edwards, T. O. Richter, W. Boer, S. Schouten, and G.-J. Brummer (2012), Sedimentation and burial of organic and inorganic temperature proxies in the Mozambique Channel, SW Indian Ocean, *Deep Sea Res., Part I*, *59*, 37–53, doi:10.1016/j.dsr.2011.10.002.

FAO/IIASA/ISRIC/ISS-CAS/JRC (2009), *Harmonized World Soil Database (version 1.1)*, FAO, Rome.

FFEM (2005), Pollution monitoring and management on the Zambezi River. Rep., French Global Environmental Facility / French Development Agency.

Franzese, A. M., S. R. Hemming, S. L. Goldstein, and R. F. Anderson (2006), Reduced Agulhas Leakage during the Last Glacial Maximum inferred from an integrated provenance and flux study, *Earth Planet. Sci. Lett.*, *250*(1–2), 72–88, doi:10.1016/j.epsl.2006.07.002.

Garcin, Y. (2008), Comment on Abrupt change in tropical African climate linked to the bipolar seesaw over the past 55,000 years by E. T. Brown, T. C. Johnson, C. A. Scholz, A. S. Cohen, and J. W. King, *Geophys. Res. Lett.*, *35*, L04701, doi:10.1029/2007GL032399.

Garcin, Y., D. Williamson, M. Taieb, A. Vincens, P.-E. Mathe, and A. Majule (2006), Centennial to millennial changes in maar-lake deposition during the last 45,000 years in tropical Southern Africa (Lake Masoko, Tanzania), *Palaeogeogr. Palaeoclimatol. Palaeoecol.*, *239*(3–4), 334–354, doi:10.1016/j.palaeo.2006.02.002.

Geological Survey of Canada (1995), Generalized geology of the world and linked databases, Ottawa, Canada.

Gärtner, A., U. Linnemann, and M. Hofmann (2014), The provenance of northern Kalahari Basin sediments and growth history of the southern Congo Craton reconstructed by U–Pb ages of zircons from recent river sands, *Int. J. Earth Sci.*, *103*(2), 579–595.

Goldstein, S., R. O'nions, and P. Hamilton (1984), A Sm–Nd isotopic study of atmospheric dusts and particulates from major river systems, *Earth Planet. Sci. Lett.*, *70*(2), 221–236.

Grantham, G., A. Manhica, R. Armstrong, F. Kruger, and M. Loubser (2011), New SHRIMP, Rb/Sr and Sm/Nd isotope and whole rock chemical data from central Mozambique and western Dronning Maud Land, Antarctica: Implications for the nature of the eastern margin of the Kalahari Craton and the amalgamation of Gondwana, *J. Afr. Earth Sci.*, *59*(1), 74–100.

Grousset, F. E., P. E. Biscaye, M. Revel, J. R. Petit, K. Pye, S. Joussaume, and J. Jouzel (1992), Antarctic (Dome C) ice-core dust at 18 ky BP—Isotopic constraints on origins, *Earth Planet. Sci. Lett.*, *111*(1), 175–182, doi:10.1016/0012-821x(92)90177-w.

Gutjahr, M., M. Frank, C. H. Stirling, V. Klemm, T. Van de Flierdt, and A. N. Halliday (2007), Reliable extraction of a deepwater trace metal isotope signal from Fe–Mn oxyhydroxide coatings of marine sediments, *Chem. Geol.*, *242*(3), 351–370.

Hauzenberger, C. A., H. Sommer, H. Fritz, A. Bauernhofer, A. Kröner, G. Hoinkes, E. Wallbrecher, and M. Thöni (2007), SHRIMP U–Pb zircon and Sm–Nd garnet ages from the granulite-facies basement of SE Kenya: evidence for Neoproterozoic polycyclic assembly of the Mozambique Belt, *J. Geolog. Soc.*, *164*(1), 189–201.

Izuka, T., I. H. Campbell, C. M. Allen, J. B. Gill, S. Maruyama, and F. Makoka (2013), Evolution of the African continental crust as recorded by U–Pb, Lu–Hf and O isotopes in detrital zircons from modern rivers, *Geochim. Cosmochim. Acta*, *107*, 96–120.

Jacobsen, S. B., and G. Wasserburg (1980), Sm–Nd isotopic evolution of chondrites, *Earth Planet. Sci. Lett.*, *50*(1), 139–155.

Jeandel, C., T. Arsouze, F. Lacan, P. Techine, and J. C. Dutay (2007), Isotopic Nd compositions and concentrations of the lithogenic inputs into the ocean: A compilation, with an emphasis on the margins, *Chem. Geol.*, *239*(1–2), 156–164, doi:10.1016/j.chemgeo.2006.11.013.

Jelsma, H. A., M. L. Vinyu, J. R. Wijbrans, E. Verdurmen, P. Valbracht, and G. Davies (1996), Constraints on Archaean crustal evolution of the Zimbabwe craton: A U–Pb zircon, Sm–Nd and Pb–Pb whole-rock isotope study, *Contrib. Mineral. Petrol.*, *124*(1), 55–70.

John, T., V. Schenk, K. Mezger, and F. Tembo (2004), Timing and PT evolution of whiteschist metamorphism in the Lufilian Arc–Zambezi Belt orogen (Zambia): Implications for the assembly of Gondwana, *J. Geol.*, *112*(1), 71–90.

Johnson, S. P., B. De Waele, F. Tembo, C. Katongo, K. Tani, Q. Chang, T. Iizuka, and D. Dunkley (2007), Geochemistry, geochronology and isotopic evolution of the Chewore–Rufunsa Terrane, Southern Irumide Belt: A Mesoproterozoic continental margin arc, *J. Petrol.*, *48*(7), 1411–1441.

Jourdan, F., H. Bertrand, U. Schärer, J. Blichert-Toft, G. Féraud, and A. Kampunzu (2007), Major and trace element and Sr, Nd, Hf and Pb isotope compositions of the Karoo large igneous province, Botswana–Zimbabwe: Lithosphere vs mantle plume contribution, *J. Petrol.*, *48*(6), 1043–1077.

Jung, S. J. A., G. R. Davies, G. M. Ganssen, and D. Kroon (2004), Stepwise Holocene aridification in NE Africa deduced from dust-borne radiogenic isotope records, *Earth Planet. Sci. Lett.*, *221*(1–4), 27–37, doi:10.1016/S0012-821X(04)00095-0.

Just, J., E. Schefuß, H. Kuhlmann, J.-B. W. Stuut, and J. Pätzold (2014), Climate induced sub-basin source-area shifts of Zambezi River sediments over the past 17 ka, *Palaeogeogr. Palaeoclimatol. Palaeoecol.*, *410*, 190–199, doi:10.1016/j.palaeo.2014.05.045.

Kolla, V., J. A. Kostecki, L. Henderson, and L. Hess (1980b), Morphology and Quaternary sedimentation of the Mozambique Fan and environs, Southwestern Indian-Ocean, *Sedimentology*, *27*(4), 357–378, doi:10.1111/j.1365-3091.1980.tb01188.x.

Kolla, V., S. Eittreim, L. Sullivan, J. A. Kostecki, and L. H. Burckle (1980a), Current-controlled, abyssal microtopography and sedimentation in Mozambique Basin, southwest Indian Ocean, *Mar. Geol.*, *34*(3–4), 171–206, doi:10.1016/0025-3227(80)90071-7.

Konecky, B. L., J. M. Russell, T. C. Johnson, E. T. Brown, M. A. Berke, J. P. Werne, and Y. Huang (2011), Atmospheric circulation patterns during late Pleistocene climate changes at Lake Malawi, Africa, *Earth Planet. Sci. Lett.*, *312*(3–4), 318–326, doi:10.1016/j.epsl.2011.10.020.

Konert, M., and J. E. F. Vandenberghe (1997), Comparison of laser grain size analysis with pipette and sieve analysis: A solution for the underestimation of the clay fraction, *Sedimentology*, *44*(3), 523–535, doi:10.1046/j.1365-3091.1997.d01-38.x.

Kröner, A., A. Willner, E. Hegner, P. Jaeckel, and A. Nemchin (2001), Single zircon ages, PT evolution and Nd isotopic systematics of high-grade gneisses in southern Malawi and their bearing on the evolution of the Mozambique belt in southeastern Africa, *Precambrian Res.*, *109*(3), 257–291.

Laskar, J., P. Robutel, F. Joutel, M. Gastineau, A. Correia, and B. Levrard (2004), A long-term numerical solution for the insolation quantities of the Earth, *Astron. Astrophys.*, *428*(1), 261–285.

März, C., J. Hoffmann, U. Bleil, G. J. de Lange, and S. Kasten (2008), Diagenetic changes of magnetic and geochemical signals by anaerobic methane oxidation in sediments of the Zambezi deep-sea fan (SW Indian Ocean), *Mar. Geol.*, *255*(3–4), 118–130, doi:10.1016/j.margeo.2008.05.013.

Meyer, I., G. R. Davies, and J.-B. W. Stuut (2011), Grain size control on Sr-Nd isotope provenance studies and impact on paleoclimate reconstructions: An example from deep-sea sediments offshore NW Africa, *Geochem. Geophys. Geosyst.*, *12*, Q03005, doi:10.1029/2010GC003355.

Möller, A., K. Mezger, and V. Schenk (1998), Crustal age domains and the evolution of the continental crust in the Mozambique Belt of Tanzania: combined Sm–Nd, Rb–Sr, and Pb–Pb isotopic evidence, *J. Petrol.*, *39*(4), 749–783.

Moore, A. E., F. P. D. Cotterill, M. P. L. Main, and H. B. Williams (2008), The Zambezi River, in *Large Rivers*, edited by A. Gupta pp. 311–332, John Wiley & Sons, Ltd.

NEN Standard 5753 (2006), Soil-determination of clay content and particle size distribution in soil and sediment by seive and pipet, Centrum voor normalisatie, Netherlands. [Available at www.nen.nl.]

Nicholson, S. E. (2000), The nature of rainfall variability over Africa on time scales of decades to millennia, *Global Planet. Change*, *26*(1–3), 137–158, doi:10.1016/s0921-8181(00)00040-0.

Partridge, T. C., P. B. Demenocal, S. A. Lorentz, M. J. Paiker, and J. C. Vogel (1997), Orbital forcing of climate over South Africa: A 200,000-year rainfall record from the Pretoria Saltpan, *Quat. Sci. Rev.*, *16*(10), 1125–1133, doi:10.1016/s0277-3791(97)00005-x.

Reason, C. J. C., W. Landman, and W. Tennant (2006), Seasonal to decadal prediction of Southern African climate and its links with variability of the Atlantic Ocean, *Bull. Am. Meteorol. Soc.*, *87*(7), 941–955, doi:10.1175/BAMS-87-7-941.

Reimer, P. J., M. G. Baillie, E. Bard, A. Bayliss, J. W. Beck, P. G. Blackwell, R. C. Bronk, C. E. Buck, G. S. Burr, and R. L. Edwards (2009), IntCal09 and Marine09 radiocarbon age calibration curves, 0–50,000 years cal BP.

Revel, M., E. Ducassou, F. Grousset, S. Bernasconi, S. Migeon, S. Revillon, J. Mascle, A. Murat, S. Zaragosi, and D. Bosch (2010), 100,000 years of African monsoon variability recorded in sediments of the Nile margin, *Quat. Sci. Rev.*, *29*(11), 1342–1362.

Ridderinkhof, H., P. M. van der Werf, J. E. Ullgren, H. M. van Aken, P. J. van Leeuwen, and W. P. M. de Ruijter (2010), Seasonal and interannual variability in the Mozambique Channel from moored current observations, *J. Geophys. Res.*, *115*, C06010, doi:10.1029/2009JC005619.

Roberts, E. M., N. J. Stevens, P. M. O'Connor, P. H. G. M. Dirks, M. D. Gottfried, W. C. Clyde, R. A. Armstrong, A. I. S. Kemp, and S. Hemming (2012), Initiation of the western branch of the East African Rift coeval with the eastern branch, *Nat. Geosci.*, *5*(4), 289–294.

Rossignol-Strick, M. (1985), Mediterranean Quaternary sapropels, an immediate response of the African monsoon to variation of insolation, *Palaeogeography, Palaeoclimatology, Palaeoecology*, *49*(3), 237–263.

Schefuss, E., H. Kuhlmann, G. Mollenhauer, M. Prange, and J. Patzold (2011), Forcing of wet phases in southeast Africa over the past 17,000 years, *Nature*, *480*(7378), 509–512.

Schneider, R., et al. (2008), Western Indian Ocean Climate and Sedimentation *Rep*.

Schneider, R. R., B. Price, P. J. Muller, D. Kroon, and I. Alexander (1997), Monsoon related variations in Zaire (Congo) sediment load and influence of fluvial silicate supply on marine productivity in the east equatorial Atlantic during the last 200,000 years, *Paleoceanography*, *12*(3), 463–481, doi:10.1029/96PA03640.

Schulz, H., A. Lückge, K.-C. Emeis, and A. Mackensen (2011), Variability of Holocene to Late Pleistocene Zambezi riverine sedimentation at the upper continental slope off Mozambique, 15°–21°S, *Mar. Geol.*, *286*(1–4), 21–34, doi:10.1016/j.margeo.2011.05.003.

Siddorn, J. R., D. G. Bowers, and A. M. Hoguane (2001), Detecting the Zambezi River Plume using observed optical properties, *Mar. Pollut. Bull.*, *42*(10), 942–950, doi:10.1016/s0025-326x(01)00053-4.

Stager, J. C., D. B. Ryves, B. M. Chase, and F. S. R. Pausata (2011), Catastrophic drought in the Afro-Asian monsoon region during Heinrich Event 1, *Science*, *331*(6022), 1299–1302, doi:10.1126/science.1198322.

Stanford, J. D., R. Hemingway, E. J. Rohling, P. G. Challenor, M. Medina-Elizalde, and A. J. Lester (2011), Sea-level probability for the last deglaciation: A statistical analysis of far-field records, *Global Planet. Change*, *79*(3–4), 193–203.

Steinhardt, J., C. Cléroux, L. de Nooijer, J. Ullgren, G.-J. Durgadoo, G.-J. Brummer, and G.-J. Reichart (2014), Anti-cyclonic eddy imprint on calcite geochemistry of several planktonic foraminiferal species in the Mozambique Channel, *Mar. Micropaleontol.*, *113*, 20–33, doi:10.1016/j.marmicro.2014.09.001.

Stumpf, R. (2011), Late Quaternary variability of hydrography and weathering inputs on the SW Iberian shelf from clay minerals and the radiogenic isotopes of neodymium, strontium and lead, PhD dissertation, Christian-Albrechts-Universität, Kiel.

Tanaka, T., S. Togashi, H. Kamioka, H. Amakawa, H. Kagami, T. Hamamoto, M. Yuhara, Y. Orihashi, S. Yoneda, and H. Shimizu (2000), JNdi-1: a neodymium isotopic reference in consistency with LaJolla neodymium, *Chem. Geol.*, *168*(3), 279–281.

Tierney, J., J. M. Russell, Y. Huang, and J. S. Sinninghe Damste (2008), Northern Hemisphere Controls on Tropical Southeast African Climate during the Past 60,000 Years, *Science*, *322*, 252–254.

Tierney, J. E., J. M. Russell, and Y. Huang (2010), A molecular perspective on Late Quaternary climate and vegetation change in the Lake Tanganyika basin, East Africa, *Quat. Sci. Rev.*, *29*(5–6), 787–800, doi:10.1016/j.quascirev.2009.11.030.

Tjallingii, R., M. Claussen, J.-B. Stuut, J. Fohlmeister, A. Jahn, T. Bickert, F. Lamy, and U. Röhl (2008), Proxy data and model simulations of sediment core GeoB7920-2, *Nat. Geosci.*, *1*, supplement, 670–675, doi:10.1038/ngeo289.

Ullgren, J. E., H. M. van Aken, H. Ridderinkhof, and W. P. M. de Ruijter (2012), The hydrography of the Mozambique Channel from six years of continuous temperature, salinity, and velocity observations, *Deep Sea Res., Part I*, *69*, 36–50, doi:10.1016/j.dsr.2012.07.003.

van der Lubbe, J. J. L., R. Tjallingii, M. A. Prins, G.-J. A. Brummer, S. J. A. Jung, D. Kroon, and R. R. Schneider (2014), Sedimentation patterns off the Zambezi River over the last 20,000 years, *Mar. Geol.*, *355*, 189–201, doi:10.1016/j.margeo.2014.05.012.

van Sebille, E., et al. (2015), Ocean currents generate large footprints in marine palaeoclimate proxies, *Nat. Commun.*, *6*, Article 6521, doi: 10.1038/ncomms7521.

Vogt, M., A. Kröner, U. Poller, H. Sommer, S. Muhongo, and M. Wingate (2006), Archaean and Palaeoproterozoic gneisses reworked during a Neoproterozoic (Pan-African) high-grade event in the Mozambique belt of East Africa: Structural relationships and zircon ages from the Kidatu area, central Tanzania, *J. Afr. Earth Sci.*, *45*(2), 139–155.

Waelbroeck, C. L. (2002), Sea-level and deep-water change derived from benthic foraminifera isotopic records, *Quat. Sci. Rev.*, *21*, 295–305.

Walford, H. L., N. J. White, and J. C. Sydow (2005), Solid sediment load history of Zambezi Delta, *Earth Planet. Sci. Lett.*, *238*, 49–63.

Wang, Y. V., T. Larsen, G. Leduc, N. Andersen, T. Blanz, and R. R. Schneider (2013), What does leaf wax δD from a mixed C3/C4 vegetation region tell us?, *Geochim. Cosmochim. Acta*, *111*, 128–139, doi:10.1016/j.gca.2012.10.016.

Weldeab, S., J. B. W. Stuut, R. R. Schneider, and W. Siebel (2013), Holocene climate variability in the winter rainfall zone of South Africa, *Clim. Past*, *9*(5), 2347–2364, doi:10.5194/cp-9-2347-2013.

Weldeab, S., D. W. Lea, H. Oberhaensli, and R. R. Schneider (2014), Links between southwestern tropical Indian Ocean SST and precipitation over southeastern Africa over the last 17 kyr, *Palaeogeogr. Palaeoclimatol. Palaeoecol.*, *410*, 200–212, doi:10.1016/j.palaeo.2014.06.001.

Ziegler, M., M. H. Simon, I. R. Hall, S. Barker, C. Stringer, and R. Zahn (2013), Development of Middle Stone Age innovation linked to rapid climate change, *Nat. Commun.*, *4*, Article 1905, doi:10.1038/ncomms2897.